Published in final edited form as:

Biochemistry. 2016 December 06; 55(48): 6673–6684. doi:10.1021/acs.biochem.6b00610.

Six Transmembrane Epithelial Antigen of Prostate 1 (STEAP1) Has a Single *b* Heme and Is Capable of Reducing Metal Ion Complexes and Oxygen

Kwangsoo Kim[†,#], **Sharmistha Mitra**[†,#], **Gang Wu**[‡,#], **Vladimir Berka**[‡], **Jinmei Song**[%], **Ye Yu**[†,&], **Sebastien Poget**[§], **Da-Neng Wang**[%], **Ah-Lim Tsai**[‡,*], **Ming Zhou**[†,*]

[†]Verna and Marrs McLean Department of Biochemistry and Molecular Biology, Baylor College of Medicine, Houston, TX 77030, USA

[‡]Division of Hematology, Department of Internal Medicine, University of Texas – McGovern Medical School, Houston, TX 77030, USA

[%]Skirball Institute of Biomolecular Medicine, New York University School of Medicine, New York, NY 10016, USA

[&]Institute of Medical Sciences and Department of Pharmacology, Shanghai Jiao Tong University School of Medicine, Shanghai 200025, China

[§]Department of Chemistry, College of Staten Island, Staten Island, NY 10314

Abstract

STEAP1, Six Transmembrane Epithelial Antigen of Prostate member 1, is highly expressed in several types of cancer cells, particularly in prostate cancer, and inhibition of its expression reduces tumor cell proliferation. However, the physiological function of STEAP1 remains unknown. Here for the first time we purified a mammalian (rabbit) STEAP1 at milligram level, enabling its high-quality biochemical and biophysical characterizations. We found that STEAP1 likely assembles as a homotrimer and forms a heterotrimer when co-expressed with STEAP2. Each STEAP1 protomer binds one heme prosthetic group which is mainly low-spin with a pair of histidine axial ligands, plus small portions of high-spin and P450 type of heme. In its ferrous state, STEAP1 is capable of reducing transition metal ion complexes of Fe^{3+} and Cu^{2+}. Ferrous STEAP1 also reacts readily with O_2 through an outer sphere redox mechanism. Kinetics with all three substrates are biphasic with ~ 80% and ~20% for the fast and slow phases, in line with its heme heterogeneity. STEAP1 retained low level of bound FAD during purification and the binding equilibrium constant, K_D, was ~ 30μM. These results highlight STEAP as a novel metal reductase and superoxide synthase, and establish a solid basis for further research into understanding of how STEAP1 activities may affect cancer progression.

Graphical Abstract

[*]Correspondence to Ming Zhou, mzhou@bcm.edu and Ah-Lim Tsai, Ah-Lim. Tsai@uth.tmc.edu.
[#]These authors contributed equally.

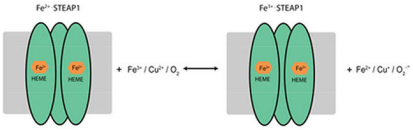

INTRODUCTION

Six Transmembrane Epithelial Antigen of Prostate (STEAP) protein was first discovered in 1999 as a cell surface antigen present in advanced metastatic prostate cancer cells (1). Subsequently, three additional homologs were identified in human genome and together they are designated as STEAP1 – 4. Among this family of proteins, STEAP1 is highly expressed in a number of human cancers including prostate, colon, bladder and liver cancers and Ewing's sarcoma. The correlation between STEAP1 expression and prostate cancer has been well documented (2). STEAP1 expression is higher in early rather than late stage of prostate cancer (3), and STEAP1 staining intensity correlates with tumor grading and appears to increase with malignancy (4). Since normal tissues have no or very little expression of STEAP1, these studies indicate that STEAP1 may play an important role in cancer progression. Yet very little is known about the functions of STEAP1.

Sequence analyses have categorized STEAP into a super family of heme-containing transmembrane ferric reductase domain (FRD), which includes yeast ferric reductase (FRE), bacterial oxidoreductase (YedZ) and human NADPH oxidases (NOX) (5, 6). FRE, NOX and all STEAP proteins have an integral membrane domain of ~150 amino acids, which is predicted to have six transmembrane (TM) helices (Fig. 1A) (5, 7). Both FRE and NOX have two pairs of conserved histidine residues in their transmembrane domains that are predicted to coordinate two heme prosthetic groups. FRE and NOX have been demonstrated to relay electrons from the intracellular side to the extracellular side, through their two heme prosthetic groups (8, 9), similar to the pair of hemes found in cytochrome b_{561} (10), mitochondrial bc_1 complex (11, 12) and photosystem II b_6f complex (13). Each STEAP isoform, on the other hand, has only one pair of conserved histidine residues per protomer and therefore is predicted to bind one heme prosthetic group each (Fig. 1A) (5, 7). These two histidine residues, His175 and His268 in STEAP1 (in both human and rabbit STEAP1 numbering), are located on the predicted TM3 and TM5, respectively (Fig. 1A). In addition to a transmembrane domain, STEAP2 – 4, but not STEAP1, have an N-terminal cytosolic domain, which has ~180 amino acids and is predicted to bind NADPH and to contribute to FAD binding (14–16) (Fig. 1A). The structural folds of the isolated cytosolic N-terminal domains from both STEAP3 and STEAP4 are similar to that of $F_{420}H_2$:$NADP^+$ oxidoreductase (FNO) (17–19), and the NADPH and FAD bindings in these cytosolic domains were characterized by biochemical studies (18, 19). Recent studies in mice and human tissues demonstrate that STEAP2 – 4 show ferric and cupric reductase activities (7, 14). A study on STEAP3-enriched cell membranes found that STEAP3 likely binds a single *b*-type heme and binds to FAD as well. Mutational studies show that residues from both the cytosolic domain and intracellular loops between transmembrane helices contribute to FAD binding (15). It is proposed that the ferric heme bound of STEAP3 – 4 is reduced by the reducing equivalent delivered from NADPH in its cytosolic domain through the bound FAD

at the interface of cytosolic and TM domains (15). These new results motivated us to provide a detailed biophysical characterization of the heme structure, and to examine whether STEAP1, the only member that does not have a cytosolic domain, has functions similar to the other STEAP isoforms (7).

In this study, we successfully over-expressed and purified a stable mammalian (rabbit) STEAP1 (rSTEAP1). The success enabled us to characterize the oligomeric state of rSTEAP1 and the stoichiometry, binding environment and redox potential of the heme prosthetic group. Our data indicate that rSTEAP1 likely forms a homotrimer but a heterotrimer when co-expressed with STEAP2. When it is reduced, ferrous STEAP1 can provide electron to ferric, cupric ions and O_2. We also demonstrated that rSTEAP1 binds FAD with an affinity significantly weaker than that of STEAP3 (15). STEAP1 thus may act as a metal reductase or a superoxide synthase with the reducing equivalent provided by the cytosolic domain of neighboring other STEAP isoforms or other cytosolic redox component(s).

MATERIALS AND METHODS

Materials.

δ-aminolevulinic acid, ferric chloride, HEPES, hemin chloride, imidazole, magnesium chloride ($MgCl_2$), potassium indigotrisulfonate (indigo), potassium ferricyanide ($K_3Fe(CN)_6$), L-tryptophan (L-Trp) and sodium hydrosulfite ($Na_2S_2O_4$) were all purchased from Sigma-Aldrich (St. Louis, MO). Phenylmethanesulfonylfluoride (PMSF) was from Amresco (Solon, OH). DNAse I was from Worthington (Lakewood, NJ). 2,2-didecylpropane-1,3-bis-β-D-maltopyranoside (MNG-DDM) was from Anatrace (Maumee, OH).

Cloning of STEAP1 constructs.

A total of 12 mammalian homologs STEAP1 were examined for their expression and stability. The full-length STEAP1 genes for each of these homologs were synthesized and subcloned into a modified pFastBac Dual vector (Invitrogen Inc., Carlsbad, CA). The genes were cloned between *Sal*I and *Not*I sites with a C-terminal Strep-tac II tags followed by an 8-histidine tag. A tobacco etch virus (TEV) protease recognition site was inserted between the C-terminus of the protein and the Strep-tac II tag. Recombinant virus particles were produced using the Bac-to-Bac protocol (Invitrogen Inc., Carlsbad, CA). Full length STEAP1 from rabbit (Accession: NP_001164745.1) showed a mono-dispersed profile in size-exclusion chromatography (20), however was unstable. Several constructs were then generated by removing the N-terminal non-structured region including the deletions from residues Glu2 to residues Asn21, Val42 or Lys70. Among these constructs, the rabbit homolog with residues 2 – 42 truncated is the most stable and therefore this construct, which we call rSTEAP1 henceforward, was used for over-expression and functional analyses of the expressed protein. Overall, rSTEAP1 is 89% identical and 94% similar to human STEAP1.

Several versions of rSTEAP1 and human STEAP2 (hSTEAP2, AAN04080.1) were constructed to test the assembly of hetero-oligomerization between STEAP1 and STEAP2.

For rSTEAP1, two versions were designed using modified pFastBac vectors: one without any tag (rSTEAP1-NT) and another one with a TEV recognition site at the C-terminus followed by an 8-histidine tag (rSTEAP1-TH). hSTEAP2 was cloned into a modified pFastBac vector with both TEV and PreScission (PrSc, GE HealthCare, Chicago, Il) recognition sequences, Strep-tac II, and 8-histidine tags in due order at the C-terminus (hSTEAP2-TPSH).

Over-expression and purification of rSTEAP1.

Bacculoviruses were generated following the manufacturer's protocol (Invitrogen). To over-express rSTEAP1, High Five™ cells (Thermo Fisher Scientific, Waltham, MA) were infected with bacculoviruses and the culture medium was supplemented with 0.5 mM δ-aminolevulinic acid, 5 μM ferric chloride and 1 μM hemin chloride. The cells were harvested 48 – 60 hours after infection and collected by centrifuging at 1000 × g for 15 minutes at 4 °C. Cell pellets were re-suspended and then spun down, twice in the hypotonic buffer (10 mM HEPES, pH 7.5 containing 10 mM NaCl, 1 mM PMSF, 5 mM $MgCl_2$ and DNAse I) and then once in the hypertonic buffer (25 mM HEPES, pH 7.5 containing 1 M NaCl, 1 mM PMSF, 5 mM $MgCl_2$ and DNAse I). The resulting crude cell membrane was re-suspended in the lysis buffer (20 mM HEPES, pH 7.5 containing 150 mM NaCl, 1 mM PMSF, 5 mM $MgCl_2$, 5 mM imidazole and 10 μM freshly prepared hemin chloride). The re-suspension was dounced 15 – 20 times and MNG-DDM was added to 1.5%. After 2 hours of gentle shaking at 4 °C, the insoluble fraction was separated by centrifugation at 55,000 × g for 60 minutes at 4 °C. The supernatant containing the detergent-solubilized protein was collected and loaded onto a Talon Co^{2+} affinity column (Clontech, Mountain View, CA) pre-equilibrated with the equilibration buffer (20 mM HEPES, pH 7.5 containing 150 mM NaCl, 0.1% MNG-DDM, 20 mM imidazole and 10 μM hemin chloride). Nonspecifically bound protein was removed by washing the resin with the same buffer. The affinity tag was removed by incubating the resin with TEV protease at 4 °C overnight. The released protein was further purified by passing through a Superdex 200 Increase 10/300 GL column (GE Health Sciences, Pittsburgh, PA) pre-equilibrated with the purification buffer (20 mM HEPES, pH 7.5 containing 150 mM NaCl and 0.01% MNG-DDM).

Co-expression and purification of rSTEAP1 and hSTEAP2.

Co-expressions of rSTEAP1 and hSTEAP2 were conducted in two ways (Fig. 2D). First, insect cells were co-infected with both rSTEAP1-NT and hSTEAP2-TPSH containing viruses, harvested, and detergent extraction was performed following a similar protocol described in the previous paragraph. The cleared supernatant was incubated with Talon Co^{2+} resin, which was washed to remove non-specifically bound proteins and then incubated with PrSc protease for 2 hours at 4°C. The resin was removed by centrifugation and the supernatant was analyzed by SDS-page and gel filtration. In this case, since only hSTEAP2 has an affinity tag, the presence of rSTEAP1 on the SDS-page would indicate co-assembly of STEAP1 and 2. Second, rSTEAP1-TH was co-expressed with hSTEAP2-TPSH. The supernatant of the cell lysate was first incubated with Strep-Tactin resin (Qiagen, Hilden, Germany) and the protein was released by incubation with PrSc protease. Since only hSTEAP2 has the Strep-Tactin tag, if rSTEAP1 and hSTEAP2 coassemble, then the release protein is a mixture of hSTEAP2 homotrimers and rSTEAP1 and hSTEAP2 heterotrimers.

Once released from the Strep-Tactin resin, hSTEAP2 no long contains any tags while rSTEAP1 still has the 8-histidine tag. The released protein was then further purified by incubating with Talon Co^{2+} resin. The protein that bound to the Talon Co^{2+} resin was then released by the TEV protease. The Talon Co^{2+} resin was subsequently removed by centrifugation and the supernatant was analyzed by SDS-page and gel filtration. The two-step purification produces pure rSTEAP1 and hSTEAP2 heterotrimers.

Multi-angle dynamic light scattering measurement.

The sample of purified rSTEAP1 (50 μL) was injected onto a Shodex KW803 analytical SEC column mounted on a Waters HPLC system (Milford, MA) and eluted with the buffer containing 0.05% MNG-DDM at a rate of 0.5 mL/min. The mass of the eluted rSTEAP1 was measured using light scattering signals recorded with a Wyatt miniDAWN TREOS 3 angle-static light-scattering detector (Santa Barbara, CA), a Wyatt Optilab rEX refractive index detector and a Waters 2489 UV absorbance detector (21). The differential refractive index (dn/dc) for MNG-DDM, 0.128 mL/g, was calculated using the Wyatt refractive index detector. The size of the protein-detergent conjugate was de-convoluted following the published method (22). In these calculations, contributions from any co-purifying lipids were not distinguished from those of MNG-DDM.

Determination of the extinction coefficients of rSTEAP1 and its heme stoichiometry.

The extinction coefficient of rSTEAP1 protein was calculated based on its A_{280} and its concentration determined using the intensity of its magnetic circular dichroism (MCD) peak at 293 nm versus a standard curve of L-Trp (23) ,based on the ratio [L-Trp]/[rSTEAP1]. The extinction coefficient of heme prosthetic group in rSTEAP1 was determined by the absorbance of its Soret band and the concentration of heme measured by the pyridine hemochrome assay (24). In the pyridine hemochrome assay, ~100 μL rSTEAP1 was first mixed with 0.15 M NaOH and 1.8 M pyridine in 750 μL and then a few grains of solid $Na_2S_2O_4$ were added. The concentration of heme was determined based on the difference spectra of the reduced and oxidized bis-pyridine heme using a difference extinction coefficient of $\Delta A_{556-538} = 24\ mM^{-1}cm^{-1}$. The heme stoichiometry was calculated as the ratio of the concentrations of heme and rSTEAP1 protein determined by L-Trp quantification.

Electronic absorption and MCD spectroscopy of rSTEAP1.

Electronic absorption spectra of rSTEAP1 were recorded using a Hewlett-Packard 8452 or 8453 diode-array spectrophotometer (Palo Alto, CA). MCD spectra of rSTEAP1 in the UV-Vis region were recorded with a Jasco J-815 CD spectropolarimeter (Tokyo, Japan). The magnetic field was provided with an Olis permanent magnet (Bogart, GA) and the field strength was calibrated with a ferricyanide solution using $A_{420} = 3.0\ M^{-1}cm^{-1}T^{-1}$. MCD measurements were conducted at room temperature at a spectral bandwidth of 5 nm, 0.5 s time constant, 0.5 nm resolution from 250 nm to 700 nm at a 200 nm/min scan speed. Each spectrum is an average of 4 repetitive scans. MCD intensity was expressed as molar difference absorption coefficient, ΔA, in units of $M^{-1}cm^{-1}$ tesla $^{-1}$.

EPR spectroscopy.

EPR spectra of the heme prosthetic group in rSTEAP1 were recorded with a Bruker EMX spectrometer at 10 K. Data analyses and spectral simulations were conducted using the WinEPR program furnished with the EMX system. The following parameters were used for the EPR measurements: frequency, 9.58 GHz; microwave power, 4 mW; modulation frequency, 100 kHz; modulation amplitude, 5 G and time constant, 0.16 s.

Measurement of midpoint potential ($E_{m,7}$) of rSTEAP1.

Midpoint potential of rSTEAP1 was measured by stoichiometric titration following the standard method with small modifications (25). The anaerobic titration vessel contained 4 μM ferric rSTEAP1 and 4 μM redox mediator indigo ($E_{m,7}$ = −71 mV), in 20 mM HEPES buffer (pH = 7.4) with 0.1 mM KCl and 0.01% MNG-DDM. Aliquots of $Na_2S_2O_4$, whose concentration was calibrated with cytochrome *c*, were added anaerobically using an air-tight Hamilton syringe (Reno, NV) and the optical changes were followed. In the reverse oxidative titrations, anaerobic solution of $K_3Fe(CN)_6$ was used to oxidize ferrous rSTEAP1. Midpoint potential of rSTEAP1 protein was calculated based on the standard Nernst equation as following equation (26):

$$E_{rSTEAP1} = -71\,mV + 59.2 \times \log\{[indigo_{ox}][rSTEAP1_{red}]/[indigo_{red}][rSTEAP1_{ox}]\} \quad [1]$$

where $[indigo_{ox}]$ and $[indigo_{red}]$ were based on the absorbance at 595 nm and extinction coefficients 15,000 $M^{-1}cm^{-1}$; $[rSTEAP1_{ox}]$ and $[rSTEAP1_{red}]$ were based on the absorbance of ferric and ferrous rSTEAP1 at 414 and 426 nm, respectively.

Stopped-flow kinetics measurements.

The reactions of ferrous rSTEAP1 with ferric or cupric ion complexes, Fe^{3+}•EDTA, Fe^{3+}•citrate and Cu^{2+}•EDTA, or O_2 were studied using an Applied Photophysics (Leatherhead, UK) model SX-18MV stopped-flow instrument, following the spectral changes using a diode-array detector and the time courses of single wavelength(s) using a monochromator to minimize photodecomposition. The sample handling unit was kept in an anaerobic chamber by Coy Lab Products, Inc. (Grass Lake, MI). Ferrous rSTEAP1 was prepared by $Na_2S_2O_4$ titration after five cycles of vacuum (30 s/cycle) and argon displacement (5 min/cycle) in a tonometer. Diode-array data were analyzed with the global analysis method using the Pro-K package (Applied Photophysics). Observed rate, k_{obs}, of single wavelength data were obtained by fitting the time courses of optical changes to the standard exponential functions:

$$A = A_0 + a_1 \times e^{(-k_{obs1} \times t)} + a_2 \times e^{(-k_{obs2} \times t)}, \quad [2]$$

where A and A_0 are the absorbance and final absorbance at equilibrium, respectively; k_{obs1} and k_{obs2} are the observed rates of the two phases; a_1 and a_2 are the amplitudes of each phase; *t* is the reaction time.

The k_{obs} of some of the rSTEAP1 reactions with Fe^{3+}•EDTA or Fe^{3+}•citrate showed linear dependence on the concentrations of ferric ion complex, the 2nd order rate constants were obtained based on the linear dependence of k_{obs} on [Fe^{3+}]:

$$k_{obs} = k_f \times \left[Fe^{3+}\right] + k_r, \quad [3]$$

where the slope represents 2nd order forward reaction constant; k_f, and the y-intercept approximates the rate constant of the reverse reaction, k_r; [Fe^{3+}] is the concentration of [Fe^{3+}•EDTA] or [Fe^{3+}•citrate].

Fluorescence titration.

Fluoresence of the rSTEAP1-bound FAD was monitored between 480 – 600 nm with an exciting wavelength of 456 nm. The bound FAD was released by boiling the protein in 1% trifluoroacetic acid (TFA) for 10 min and the denatured protein was removed by centrifugation. The fluorescence of the supernatant was compared to that of free FAD of known concentration in buffer. The affinity of rSTEAP1 for FAD was estimated by progressively adding FAD into a buffer with or without rSTEAP1 and monitoring the fluorescence at 510 nm. The difference of FAD fluorescence with and without rSTEAP1, $\Delta F_{510} = F_{buffer/FAD} - F_{rSTEAP1/FAD}$, was plotted versus FAD concentrations.. The dissociation constant, K_D of FAD, was obtained by fitting the isotherm with a standard hyperbola function:

$$\Delta F = \Delta F_{max} \times [FAD]/(K_D + [FAD]). \quad [4]$$

RESULTS AND DISCUSSIONS

Oligomeric state of rSTEAP1.

rSTEAP1 was expressed using the bacculovirus expression system and yielded ~3 mg of pure proteins from 1 liter of cell culture (Methods). The purified rSTEAP1 is stable and thus suitable for biochemical and biophysical characterizations.

The purified rSTEAP1 protein has a major band migrating to between the 25 and 35 kDa molecular weight markers on a SDS-PAGE gel (Fig. 1C, Lane 2). The purified rSTEATP1 was cleaved off the metal affinity column by TEV, and the enzymatic cleavage was complete as indicated by the absence of rSTEAP1 on the affinity resin after TEV treatment (Fig. 1C, Lane 3). The protein band in Lane3 is TEV protease (~25kDa), because it has a 6-histidine tag and binds to the affinity column. In addition to the major band, purified rSTEAP1 protein has two minor bands on a SDS-PAGE migrating to molecular weights corresponding to approximately two and three times that of the rSTEAP1 protomer. (Fig. 1C, Lanes 2 and 4). The higher molecular weight species suggest that rSTEAP1 may exist as a homotrimer or higher order oligomers, and that the oligomeric state is partially resistant to the denaturing conditions in SDS-PAGE. The purified rSTEAP1 was further analyzed by size-exclusion chromatography and rSTEAP1 elutes as a single symmetrical peak (Fig. 1D), indicating that the sample is monodisperse. The elution volume of the purified rSTEAP1 is close to another membrane protein MalT, which is known to form a homodimer and the dimer has a

molecular weight of 102 kDa (Fig. 1D, inset and ref (27)). Thus rSTEAP1 likely forms a trimer. The oligomeric state of rSTEAP1 was further investigated using size-exclusion chromatography in combination with multi-angle light scattering method (SEC-MALS) and the SEC-MALS measurement showed that rSTEAP1 has a molecular weight of ~110 kDa (Fig. 2A), consistent with the conclusion that rSTEAP1 forms a trimer.

Our conclusion of a trimeric rSTEAP1 is not in direct conflict with the data from previous studies that suggest STEAP3 and 4 could form dimers (15, 18, 19). In one study, a green fluorescence protein (GFP) was split into two complementary halves and each half was individually fused to a STEAP3; GFP fluorescence was observed when the two STEAP3 fusion proteins were co-expressed, leading to the conclusion that STEAP3 forms a dimer (15). However, these data are compatible with a trimeric assembly as well. In other studies, the cytosolic domains of STEAP3 and STEAP4 were found to form dimers of a similar interface (18, 19), lending support to a dimeric assembly of the two full length proteins. However the interactions of isolated soluble domains may not always reflect that of the transmembrane domains.

We then studied whether rSTEAP1 can form hetero-oligomer(s) with other STEAP isoform(s). Since overexpression of rabbit STEAP2 was not successful, human STEAP2 (hSTEAP2) was tested and the amino acid sequence of hSTEAP2 is 96% identical to that of rabbit STEAP2. First, a rabbit STEAP1 construct with no affinity tag (rSTEAP1-NT) was co-expressed with hSTEAP2 that has an 8-histidine affinity tag and a Strep-tac II tag (hSTEAP2-TPSH). The two tags can be cleaved by the PreScission protease (Fig. 2D). Co^{2+} chelating resin was used to isolate proteins with a histidine affinity tag and SDS-PAGE analysis showed that the purified protein contains both rSTEAP1 (35 kDa) and hSTEAP2 (56 kDa) (Fig. 2B, Lane 3), indicating that the two proteins co-assemble. Second, a rabbit STEAP1 construct with an 8-histidine tag was co-expressed with hSTEAP2-TPSH, and Strep-Tactin resin was used to purify proteins that has a Strep-tac II tag and the purified protein was cleaved off the resin using the Precission protease (Fig. 2D). As expected, both rSTEAP1 and hSTEAP2 were present (Fig. 2B, lane 4). Co^{2+} chelating resin was then used to further purify the proteins with a His tag, and the purified protein has both rSTEAP1 and hSTEAP2 (Fig. 2B, Lane 5). The doubly purified protein eluted as a single peak on a size-exclusion column (Fig. 2B, Lanes 6 – 9). The FPLC of co-expressed rSTEAP1/hSTEAP2 showed a major fraction eluted at volume similar to rSTEAP1 homotrimer, consistent with formation of a heterotrimer between rSTEAP1 and hSTEAP2 (Fig. 1B and 2C). Although the current experiment does not allow us to resolve whether the heterotrimer is composed of two STEAP1 and one STEAP2 or the other way around, the ability of STEAP1 to form hetero oligomer with other STEAP isoform(s) may have important implications for its functions.

Electronic absorption and MCD spectroscopy of rSTEAP1.

We next characterized the heme prosthetic group in rSTEAP1. A UV-Vis absorption spectrum of purified rSTEAP1 showed a Soret peak at 412 nm, with an extinction coefficient of 117.3 $mM^{-1}cm^{-1}$, and a broad α/β band centered at 550 nm (Fig. 3A). The heme stoichiometry in rSTEAP1 was further analyzed with pyridine hemochrome method, which

indicates a non-covalently bound *b* type heme with a 1.00 ± 0.05 heme per rSTEAP1 protomer (n = 3). Addition of 250 mM imidazole (Im) to ferric rSTEAP1 did not introduce any shift of its Soret peak but only a slight increase in extinction coefficient, indicating a major population of low-spin heme in purified rSTEAP1 and only small amount high-spin heme which can be converted to low-spin by imidazole. Upon reduction with $Na_2S_2O_4$, ferrous rSTEAP1 exhibited a Soret peak at 426 nm with an extinction coefficient of 187.1 $mM^{-1}cm^{-1}$ and split α and β bands, at 560 nm (32.7 $mM^{-1}cm^{-1}$) and 530 nm (17.2 $mM^{-1}cm^{-1}$), respectively, consistent with a bis-imidazole *b*-type cytochrome (Fig. 3A).

rSTEAP1 was further characterized using MCD spectroscopy. Consistent with UV-Vis spectroscopy, MCD spectrum of ferric rSTEAP1 confirms a majorly low-spin heme by the strong Soret signals between 403 nm (150.2 $M^{-1}cm^{-1}Tesla^{-1}$) to 418 nm (−195.5 $M^{-1}cm^{-1}Tesla^{-1}$) and a crossover at 410 nm, the presence of a trough at 569 nm of −16.0 $M^{-1}cm^{-1}Tesla^{-1}$ and no high-spin charge-transfer signal at wavelength above 600 nm (Fig. 3B) (28). As in UV-Vis spectroscopy, addition of imidazole only caused slight increase in intensity but no shift for the Soret peak in the MCD spectrum of ferric rSTEAP1 (Fig. 3B), consistent with that the majority of heme in ferric rSTEAP1 is in low-spin state. The MCD spectrum of ferrous rSTEAP1 exhibited a very strong α band of 387.5 $M^{-1}cm^{-1}Tesla^{-1}$ at 552 nm to −423 $M^{-1}cm^{-1}Tesla^{-1}$ at 559 nm with crossover at 555 nm, and a β band between 525.5 nm (19.0 $M^{-1}cm^{-1}Tesla^{-1}$) and 531.5 nm (−28.5 $M^{-1}cm^{-1}Tesla^{-1}$) with crossover at 528 nm (Fig. 3B), consistent with the intense A-term Faraday effect of typical low-spin *b* type heme (28). This intense Aterm MCD signal is one of the largest ever reported. Compared to that of ferric rSTEAP1, the Soret band of ferrous rSTEAP1 was significantly weaker (Fig. 3B). The spin state of heme in rSTEAP1 therefore remains mainly in low-spin state at different redox states.

EPR characterization of rSTEAP1.

Expression and purification of rSTEAP1 to mg level enabled for the first time the characterization of the spin state(s) of the heme in ferric rSTEAP1 using EPR spectroscopy (Fig. 4). Consistent with the UV-Vis and MCD data, significant EPR signatures for low-spin ferric heme were observed for ferric rSTEAP1 (Fig. 4A). The principal g values of the rhombic low-spin heme, $g_{z/y}$ = 3.37/2.26 and a very small g_x, are consistent with those of highly axial low-spin heme (HALS) (29, 30). The HALS type heme geometry is likely held by constrains exerted by rSTEAP1 protein. Interestingly, EPR spectrum revealed additional set of low-spin heme EPR signatures, observed at g values of 2.43, 2.26 and 1.90 (Fig. 4A), suggesting the existence of some P450-like heme. EPR signatures due to high-spin heme were also observed for ferric rSTEAP1. Moreover, the high-spin signal was heterogeneous, containing both rhombic component, with g_x = 6.73 and g_y = 5.00, and axial component, with g_x/g_y = 6.01. The g_z for both high-spin heme geometries was observed at ~2.0 (Fig. 4A). However, it is hard to quantify the relative amounts of high- and low-spin hemes since the EPR signals for low-spin heme are usually much weaker than those of high-spin heme (the so called g-strain).

Formation of ferric STEAP1-Im complex abolished most of the high-spin heme signals, leading to a predominant low-spin heme with three principal g values at 2.94, 2.26 (Fig. 4B)

and 1.52 (unrecognizable in the obtained EPR spectrum), indicating the formation of a 6 coordinate (6c) bis-imidazole heme complex (Im-Fe-His). The g values, 3.33/2.26 of ferric rSTEAP1-Im, were essentially the same as those of the resting low-spin ferric rSTEAP1: 3.37/2.26 (Fig. 4B), indicating that the axial ligand field and the rhombicity of heme in ferric rSTEAP1-Im complex are very similar to those in low-spin ferric rSTEAP1. The original distal histidine ligand in ferric low-spin rSTEAP1 is not replaced by imidazole. However, evolvement of the 2.94 signal and enhancement of the 2.26 signal after imidazole addition appeared to match the disappearance of the high-spin heme signals. As this distal imidazole ligand in the new low-spin heme is not bonded to the protein, it is present as a non-strained form and not a HALS heme. Interestingly, EPR signals due to the P450-like heme were still as visible as in rSTEAP1 in the presence of imidazole (Fig. 4B), indicating imidazole is not capable of replacing the cysteine thiolate proximal ligand in the P450-like heme either. The origin of P450 type heme signals is unclear. However, since excess imidazole did not replace the cysteine ligand to heme, this ligand is most likely a part of rSTEAP1 protein. Rabbit STEAP1 has only two cysteine residues: Cys57 and Cys312. Cys312 in our rSTEAP1 construct is predicted to be at the end of the sixth TM helix, thus may not be flexible enough to ligate the heme iron. In contrast, Cys57 is predicted to locate in a flexible cytosolic loop before the first TM helix and should be a good candidate to serve as a heme ligand. Cys57 is conserved in human STEAP1, although it is not conserved in STEAP 2 – 4, which contains some other cysteines (14). It will be interesting to examine whether the P450 type heme is indeed due to Cys 57 and whether this plays a biological role.

Overall, our characterization of rSTEAP1 indicates that heme coordination in rSTEAP1 is heterogeneous, which likely reflects the flexible structure of rSTEAP1. Such heterogeneity in heme coordination may be a general phenomenon in single-heme transmembrane proteins and will be assessed in other STEAP isozymes. However, structural perturbation during purification, particularly during detergent solubilization, cannot be excluded at this stage.

Midpoint potential of rSTEAP1.

The rigid heme geometry detected in rSTEAP1, as indicated by its EPR signatures of a HALS type heme, suggests an electron transfer function for STEAP1, since the HALS type of low-spin heme is unanimously found to function as redox centers for efficient electron-transfer. This type of heme is typical for those two-heme *b* cytochromes found in strict electron-transfer systems such as PSII, b_6f, NOX and cytochrome b_{561}. We therefore assessed the redox role of rSTEAP1 by determining its midpoint potential, $E_{m,7}$. However, an unexpected obstacle was encountered because rSTEAP1 aggregated in the presence of excess redox dyes (10 – 25 μM) in our potentiometric titration, including two sets of dyes tested: 2-OH-1,4-naphtoquinone (−152 mV)/indigo blue (−45 mV)/methylene blue (+11 mV)/1,4-naphtoquinone (+60 mV) and indigo blue (−45 mV)/duroquinone (+5 mV)/ phenazine methosulfate (+80 mV) (values in parentheses: midpoint potentials of the dyes) (25). The hurdle was bypassed using stoichiometric titration in the presence of stoichiometric level of a single reference dye, indigo. Indigo has an $E_{m,7}$ of −71 mV (31, 32) and provided a good reference for the relative potential to that of rSTEAP1 in each titration.

During the anaerobic reduction of 1:1 mixture of rSTEAP1/indigo with $Na_2S_2O_4$, the Soret peak of rSTEAP1 gradually shifted from 412 nm to 428 nm with clear isosbestic points at 418 nm and 441 nm (Fig. 5), together with the decrease of indigo's absorbance at 595 nm. rSTEAP1 and indigo each exhibited minimal absorbance at 595 nm and at heme Soret region, respectively, this clean optical separation allowed calculation of the degree of reduction for STEAP1 and indigo individually (Fig. 5, inset). After full reduction, the same rSTEAP1 sample was oxidized by reverse titration with anaerobic $Fe(CN)_6^{3-}$ (data not shown). The UV-Vis spectra of rSTEAP1 remained unchanged after the reduction/oxidation titration cycle indicating that rSTEAP1 can be reversibly reduced and oxidized. The redox potentials determined from two different batches of rSTEAP1 based on Eq. [1] with eight pairs of relative extent of reduction (oxidation) between rSTEAP1 and indigo were −114.9 ± 7.8 mV and −118.4 ± 8.4 mV for the reductive (Fig. 5, inset) and oxidative paths (data not shown), respectively.

Reductions of ferric and cupric ion complexes by ferrous rSTEAP1.

The redox potential of rSTEAP1, −114 – −118 mV, suggests that it may be functional in reducing ferric and cupric ions existing in various forms of coordinated complexes physiologically. The reactivity of ferrous rSTEAP1 with some of these metal ion complexes were assessed for the oxidative part of the overall redox reaction under single-turnover conditions. Spectral changes of rSTEAP1 were first studied using rapid-scan stopped-flow method during its reactions with ferric ions chelated with EDTA (Fe^{3+}.EDTA) or citrate (Fe^{3+}.citrate) and cupric ion chelated with EDTA (Cu^{2+}.EDTA) (Fig. 6). Among these three substrates, Fe^{3+}•citrate is likely physiologically relevant, due to the abundance of both Fe^{3+} and citrate *in vivo*. The EDTA complexes of ferric and cupric ions, although unlikely found in any significant amounts *in vivo*, may also be structurally similar to other complex metal ions found physiologically.

When ferrous rSTEAP1 was mixed anaerobically with either Fe^{3+}•EDTA (Fig. 6A) or Fe^{3+}•citrate (Fig. 6B), its Soret peak exhibited hypsochromic shift with clear isosbestic points at 418 nm, 441 nm and 569 nm. The final wavelength of Soret peak was 412 nm and no reaction intermediate was observed (Fig. 6A and B), indicating a one-step process in both reactions. Oxidation of ferrous rSTEAP1 by 250 μM Fe^{3+}•EDTA was complete within 50 ms (Fig. 6A) and required 110 ms for 250 μM Fe^{3+}•citrate (Fig. 6B). On the other hand, when ferrous rSTEAP1 was reacted with 500 μM Cu^{2+}•EDTA, the Soret peak only shifted to 422 nm with a shoulder at 415 nm after 197 s, indicating that rSTEAP1 was only partially oxidized by Cu^{2+}•EDTA (Fig. 6C). The oxidation rate of ferrous rSTEAP1 therefore clearly showed dependence on the chemical structures of the metal ion complexes (Fig. 6). The isosbestic points of ferrous rSTEAP1/Cu^{2+}•EDTA reaction were observed at 418 nm, 441 nm and 558 nm, same as those observed for rSTEAP1 oxidation by ferric ion complexes (Fig. 6A and B) and no spectral intermediate was observed in the reaction between ferrous rSTEAP1 and Cu^{2+}•EDTA either (Fig. 6). The different reaction rates highlight the specificity of rSTEAP1 for different ions and its potential function as a metal reductase.

The optical properties of both rSTEAP1 and metal ion complexes changed after long exposure to white light used in rapid-scan optical characterization. To measure the slow

oxidation kinetics of ferrous rSTEAP1 by Cu^{2+}•EDTA, the reaction was further studied by single wavelength stopped-flow to obtain kinetics of A_{426}, the peak of ferrous rSTEAP1 (Fig. 7A). The much faster reactions between rSTEAP1 and Fe^{3+}•EDTA or Fe^{3+}•citrate were also studied using single wavelength stopped-flow since more time points can be collected in millisencond region than rapid scan diode array (Fig. 7A). The reaction with each metal ion complex exhibited a biphasic kinetics (Fig. 7A), but the observed rates, k_{obs}'s, exhibited different [metal ions] dependence (Fig. 7B – D). Fe^{3+}•EDTA oxidized rSTEAP1 with the fastest rate (Fig. 7B). The fast phase, accounted for ~80% of the total ΔA_{426}, and the slow phase, accounted for the rest (Fig. 7B). The k_{obs}'s of both phases exhibited linear dependence on [Fe^{3+}•EDTA] (Fig. 7B), and k_f/k_r obtained based on Eq. [3] were: $2.7 \times 10^5\ M^{-1}s^{-1}$ and $4.8\ s^{-1}$ for the fast phase; and $4.0 \times 10^4\ M^{-1}s^{-1}$ and $1.4\ s^{-1}$ for the slow phase, respectively (Fig. 7B). Similar to Fe^{3+}•EDTA, Fe^{3+}•citrate oxidized rSTEAP1 biphasically, with a fast phase (~ 80% the total change) k_{obs} exhibiting linear dependence on [Fe^{3+}•citrate], but the slow phase (~20%) exhibited a saturation phenomenon (Fig. 7C). Rate constants k_f and k_r obtained were $1.6 \times 10^5\ M^{-1}s^{-1}$ and $15.5\ s^{-1}$, respectively for the fast phase (Fig. 7C). The saturable dependence of the slow phase can be fit with a saturable hyperbolic function similar to equation [4]:

$$k_{obs} = k_{max} \times \left[Fe^{3+} \bullet \text{citrate}\right] / \left(K_M + \left[Fe^{3+} \bullet \text{citrate}\right]\right) \quad [5]$$

to yield k_{max} of $11.5\ s^{-1}$ and K_M of 46.3 μM (Fig. 7C). Cu^{2+}•EDTA also oxidized ferrous rSTEAP1 in a biphasic manner, however, the k_{obs} of the fast phase showed independence of [Cu^{2+}•EDTA], with an average of ~ $0.39\ s^{-1}$ (Fig. 7D). The k_{obs} of the slow phase, however, exhibited a saturable behavior, with a k_{max} of $0.024\ s^{-1}$ and a K_M of 1.5 mM (Fig. 7D).

The single-turnover biphasic reduction kinetics (Fig. 7) are due to the heterogeneity of rSTEAP1 sample having two intrinsically different electron transfer rates, accounting for ~80% (fast phase) and ~ 20% (slow phase) populations, respectively. This kinetic heterogeneity corroborates the EPR data indicating that the heme is present at different spin-states or/and with different axial ligands, such as P450 type coordination (Fig. 4). Combining spectroscopic characterization (Figs. 3 and 4) and the transient kinetics (Figs. 6 & 7), it is easy to correlate the fast phase kinetics to the 6c low-spin heme and the slow phase to the high-spin or P450 type heme.

The linear dependence of k_{obs} on [Fe^{3+}•EDTA] in both phases and on [Fe^{3+}•citrate] in the fast phase can be interpreted as a hybrid of two mechanisms: (A) an efficient direct outer sphere, one-step electron transfer:

$$\text{Fe(II)rSTEAP1} + Fe^{3+}\left(\text{or}\,Cu^{2+}\right) \leftarrow\rightarrow \text{Fe(III)rSTEAP1} + Fe^{2+}\left(\text{or}\,Cu^{1+}\right) \quad (1)$$

or (B) a two-step mechanism involving a first binding step (2a) followed by prompt electron transfer (2b):

$$\text{Fe(II)rSTEAP1} + Fe^{3+}\left(\text{or}\,Cu^{2+}\right) \leftarrow\rightarrow \text{Fe(II)rSTEAP1}/Fe^{3+}\left(\text{or}\,Cu^{2+}\right) \quad (2a)$$

$$\mathrm{Fe(II)rSTEAP1/Fe^{3+}\left(or\,Cu^{2+}\right)} \rightarrow \mathrm{Fe(III)rSTEAP1 + Fe^{2+}\left(or\,Cu^{1+}\right)} \quad (2b)$$

In both mechanisms, the step of direct electron-transfer (reaction 1) or binding (reaction 2a) of ferric ions with ferrous rSTEAP1 is rate-limiting and its rate is linearly dependent on [ferric ion] (Fig. 7A). Analysis based on mechanism A, the k_f/k_r are 2.7×10^5 $M^{-1}s^{-1}/4.8$ s^{-1} (fast phase) and 4.0×10^4 $M^{-1}s^{-1}/1.4$ s^{-1} (slow phase) for Fe^{3+} •EDTA and 1.6×10^5 $M^{-1}s^{-1}/15.5$ s^{-1} (fast phase) for Fe^{3+}•citrate. In contrast, analysis based on the two-step model, the binding affinity constants can be calculated as $K_D = k_r/k_f$, 17.8 μM and 35 μM, of Fe^{3+}•EDTA reaction for the two rSTEAP1 populations; and 96.9 μM of Fe^{3+}•citrate reaction for ~80% of rSTEAP1, respectively. In the cases of slower electron transfer, k_{obs}'s either showed independence on [metal ion] (mechanism A), such as the fast phase reaction with Cu^{2+}•EDTA, or a Michaelis-Menten type saturable kinetics (mechanism B), observed in the slow phase of the reactions with either Fe^{3+}•citrate or Cu^{2+}•EDTA. About 80% ferrous rSTEAP1 reduced Cu^{2+}•EDTA at 0.39 s^{-1} and ~20% ferrous rSTEAP1 reacted slowly with Fe^{3+}•citrate or Cu^{2+}•EDTA, the maximum electron transfer rates, k_{max}, were 11.5 s^{-1} and 0.024 s^{-1}, respectively. However, a K_M obtained from eq. [5] is different from true Michaelis-Menten K_M since the metal ion reductions in this study were conducted under single turnover conditions and never reached steady state. Nonetheless, K_M's obtained from eq. [5] reflect the affinities of the minor population of rSTEAP1 for Fe^{3+}•citrate or Cu^{2+}•EDTA.

Reactions of O_2 with ferrous rSTEAP1.

Other than reducing metal ion complexes, the low redox potential of rSTEAP1 suggests that ferrous rSTEAP1 is capable of reducing O_2. We investigated the kinetics of this reaction by reacting anaerobic ferrous rSTEAP1 with O_2. The Soret peak shifted from 428 nm to 412 nm with clear isosbestic points at 418 nm, 441 nm, 521 nm and 570 nm (Fig. 8A). These spectral changes are essentially the same as those observed during the reaction of ferrous rSTEAP1 with Fe^{3+}•EDTA. No spectral intermediate was resolved from the kinetic data, indicating that oxyferrous rSTEAP1 did not form or quickly converted to ferric rSTEAP1.

The oxidation rate of ferrous rSTEAP1 by O_2 was then measured more accurately by following the time courses of A_{426}. The kinetics exhibited biphasic exponential decay (data not shown). The fast and slow phases again accounted for ~80% and ~20% of the total A_{426} change, respectively, similar to that observed in the reactions of ferrous rSTEAP1 with ferric or cupric ion complexes. As deciphering the reactions with metal ion complexes, O_2 reacts with the 6c low-spin heme in the fast phase (~80% of observed ΔA_{426}). The rate constant k_{obs1}, for the fast phase, was measured to be ~0.9 s^{-1} at all levels of [O_2] (Fig. 8B), and k_{obs2}, for the slow phase, exhibited a saturable dependence on [O_2]. The k_{max} of this slow phase reached 0.18 s^{-1} with a K_M = 15 μM (Fig. 8B). As in the metal ion reduction study, here K_M reflects the affinities of the minor population of rSTEAP1 for O_2.

Similar to the two possible mechanisms of the reactions with metal ion complexes (reactions 1 and 2), biphasic kinetics of ferrous rSTEAP1 with O_2 can be interpreted by either (A) a

fast direct outer sphere, one-step electron transfer from ferrous rSTEAP1 to O_2, represented by the following reaction,

$$\mathrm{Fe(II)rSTEAP1} + \mathrm{O_2} \leftarrow\ \rightarrow \mathrm{F(III)rSTEAP1} + \mathrm{O_2^{\bullet\ -}} \quad (3)$$

or (B) a two-step mechanism involving a first binding step (4a) followed by prompt electron transfer (4b):

$$\mathrm{Fe(II)rSTEAP1} + \mathrm{O_2} \leftarrow\ \rightarrow \mathrm{Fe(II)rSTEAP1 - O_2} \quad (4a)$$

$$\mathrm{Fe(II)rSTEAP1 - O_2} \rightarrow \mathrm{Fe(III)rSTEAP1} + \mathrm{O_2^{\bullet\ -}} \quad (4b)$$

Since the fast phase of O_2 oxidation is independence of [O_2] (Fig. 8B), ferrous rSTEAP1 with 6c low-spin heme likely reacts with O_2 through mechanism A (reaction 3). On the other hand, since the slow oxidation follows a Michaelis-Menten type kinetics, O_2 likely binds to ferrous rSTEAP1 first (4a) before electron transfer (4b). O_2 may initially bind to high-spin ferrous heme or the P450 type heme. However, since no oxyferrous heme intermediate was observed during the reaction, O_2 more likely binds to a site other than heme. The slow reaction phase between ferrous rSTEAP1 and O_2 is therefore also an outer sphere electron transfer process.

Binding of FAD with rSTEAP1.

Reduction of metal ion complexes and oxygen by ferrous rSTEAP1 *in vivo* is expected to be dependent upon the initial electron transfer to its heme. In STEAP2 – 4, an electron transfer pathway is proposed as follows: NADPH (cytosolic domain) → FAD (cytosolic domain and αII/III and αIV/V loops) → heme (TM domain) → substrate (15, 18). STEAP1, although does not possess a cytosolic domain, has conserved intracellular loops and was hypothesized to bind FAD (15). We therefore examined whether the purified rSTEAP1 contained FAD. Although FAD has a significantly smaller extinction coefficient than that of heme, which may lead to no distinct FAD absorption in rSTEAP1's UV-Vis spectrum (Fig. 2A), it may be detected by its fluorescence since heme does not fluoresce. Excited at 456 nm, the purified rSTEAP1 exhibited a broad fluorescence emission between 480 to 600 nm peaked at 510 nm (Fig. 9A), indicating that it likely contains bound FAD. However, only ~0.4 μM FAD was released from 23.3 μM denatured rSTEAP1, estimated by comparing the fluorescence of the released FAD with that of free FAD standard (Fig. 9A). This indicates that rSTEAP1 may have low affinity to FAD and most of the FAD was lost during rSTEAP1 purification. The fluorescence of the released FAD was significantly stronger than that of rSTEAP1-bound FAD (Fig. 9A), indicating that the fluorescence of rSTEAP1-bound FAD is quenched by neighboring heme. The reduction in fluorescence upon binding to rSTEAP-1 was used to estimate the affinity of FAD to rSTEAP1 by titrating either rSTEAP1 or buffer with FAD and following the change of fluorescence at 510 nm, $\Delta F_{510} = F_{\mathrm{buffer/FAD}} - F_{\mathrm{rSTEAP1/FAD}}$, versus [FAD] (Fig. 9B). Fitting the data points with a simple binding isotherm (eq. [4]) yielded an apparent K_D of 32.3 ± 1.3 μM (Fig. 9B). The affinity of rSTEAP1 for FAD is

therefore much lower than that of STEAP3 (15), consistent with the notion that FAD interact with both the intracellular domain and the loops from the transmembrane domain (15).

CONCLUSIONS

Our success in producing sufficient amount of rSTEAP1 enabled the first high-quality biochemical/biophysical characterization of STEAP1, which is representative of the transmembrane domains of all STEAPs. Our data show that the purified rSTEAP1 likely forms a homotrimer, also capable of forming a heterotrimer with other STEAP isoform(s). Each rSTEAP1 protomer binds one heme, whose association to rSTEAP1 protein is heterogeneous. Majority of rSTEAP1 ligates to form 6c low-spin heme through a pair of conserved histidines. The geometry of the 6c low-spin heme is rigid. Minor portion of rSTEAP1 binds a high-spin heme through one proximal histidine or a P450 type of heme with a proximal cysteine. The midpoint potential of rSTEAP1, $E_{m,7}$, was measured −114 – −118 mV. Moreover, rSTEAP1 exhibits an affinity of ~32 μM for FAD. These biophysical properties of rSTEAP1 render it a decent reductant for several metal ion complexes and O_2, analogous to those found for FRD and NOX *in vivo* activities. In STEAP 2 – 4, it is proposed that electron transfers from NADPH through FAD and heme to metal ions (7, 14). For STEAP1, although it does not have a cytosolic NADPH/FAD binding domain, electrons may be transferred in a pathway similar to those in other STEAP isoforms: NADPH (neighboring STEAP isoform(s)/other oxidoreductase protein/domain) → FAD (STEAP1 or other STEAP isoforms) → heme (STEAP1) → metal ions/O_2 (Fig. 1B). This electron pathway renders STEAP a unique family of metal reductase/superoxide synthase, which transfers electron through only one heme, while FRD and NOX have two hemes each to operate (6, 33, 34).

Overall, STEAP1, other than being a biomarker of different cancers, may play roles in metal metabolism or generation of superoxide by one-electron reduction of O_2. The latter could be an attribute for its role in mediating cancer (or inflammation) (35). Our foundational biochemical and biophysical studies on STEAP1 warrant further in-depth studies to decipher the molecular mechanism for the function of this protein in carcinogenesis.

Funding Sources

This work was supported by the National 973 Program from the Chinese Ministry of Science and Technology (2014CB910301) to Y.Y. and M.Z.; National Institutes of Health HL086392, GM098878, and DK088057 to M.Z. and NS094535 to A.T., American Heart Association 12EIA8850017 to M.Z., and Cancer Prevention and Research Institute of Texas R1223 to M.Z.

Abbreviations:

b_6f	cytochrome *b6f* complex
EPR	electron paramagnetic resonance spectrometry
FNO	$F_{420}H_2$:$NADP^+$ oxidoreductase
FRE	ferric reductase

GFP	green fluorescence protein
HALS	highly axial low-spin heme
STEAP1	Six Transmembrane Epithelial Antigen of Prostate member 1
hSTEAP2	human STEAP2
hSTEAP2-TPSH	hSTEAP2 with Strep-tac II and 8-histidine tags in due order at the C-terminus
PrSc	PreScission protease
MCD	magnetic circular dichroism
MNG-DDM	2,2-didecylpropane-1,3-bis-β-D-maltopyranoside
NOX	human NADPH oxidase
PSII	photosystem II
rSTEAP1	2 – 42 truncated STEAP1
rSTEAP1-NT	rSTEAP1 without His tag
rSTEAP1-TH	rSTEAP1 with TEV recognition site followed by an 8-histidine tag at the C-terminus
hSEAP2-TPSH	human STEAP2 with TEV recognition site followed by a C-terminal Strep-tac II tag and an 8-histidine tag
SEC	size-exclusion chromatography
SEC-MALS	size-exclusion chromatography with multi-angle light scattering analysis
TEV	tobacco etch virus
YedZ	bacterial oxidoreductase

REFERENCES

1. Hubert RS, Vivanco I, Chen E, Rastegar S, Leong K, Mitchell SC, Madraswala R, Zhou Y, Kuo J, Raitano AB, Jakobovits A, Saffran DC, and Afar DE (1999) STEAP: a prostate-specific cell-surface antigen highly expressed in human prostate tumors, Proc Natl Acad Sci U S A 96, 14523–14528. [PubMed: 10588738]
2. Bret C, Klein B, and Moreaux J (2012) Gene expression-based risk score in diffuse large B-cell lymphoma, Oncotarget 3, 1700–1710. [PubMed: 23482333]
3. Gomes IM, Arinto P, Lopes C, Santos CR, and Maia CJ (2014) STEAP1 is overexpressed in prostate cancer and prostatic intraepithelial neoplasia lesions, and it is positively associated with Gleason score, Urol Oncol 32, 53 e23–59.
4. Ihlaseh-Catalano SM, Drigo SA, de Jesus CM, Domingues MA, Trindade Filho JC, de Camargo JL, and Rogatto SR (2013) STEAP1 protein overexpression is an independent marker for biochemical recurrence in prostate carcinoma, Histopathology 63, 678–685. [PubMed: 24025158]

5. Zhang X, Krause KH, Xenarios I, Soldati T, and Boeckmann B (2013) Evolution of the ferric reductase domain (FRD) superfamily: modularity, functional diversification, and signature motifs, PLoS One 8, e58126. [PubMed: 23505460]
6. Finegold AA, Shatwell KP, Segal AW, Klausner RD, and Dancis A (1996) Intramembrane bis-heme motif for transmembrane electron transport conserved in a yeast iron reductase and the human NADPH oxidase, J Biol Chem 271, 31021–31024. [PubMed: 8940093]
7. Ohgami RS, Campagna DR, Greer EL, Antiochos B, McDonald A, Chen J, Sharp JJ, Fujiwara Y, Barker JE, and Fleming MD (2005) Identification of a ferrireductase required for efficient transferrin-dependent iron uptake in erythroid cells, Nat Genet 37, 1264–1269. [PubMed: 16227996]
8. Fujii H, Finnegan MG, and Johnson MK (1999) The active form of the ferric heme in neutrophil cytochrome b(558) is low-spin in the reconstituted cell-free system in the presence of amphophil, J Biochem 126, 708–714. [PubMed: 10502679]
9. Doussiere J, Gaillard J, and Vignais PV (1996) Electron transfer across the O2- generating flavocytochrome b of neutrophils. Evidence for a transition from a low-spin state to a high-spin state of the heme iron component, Biochemistry 35, 13400–13410. [PubMed: 8873608]
10. Lu P, Ma D, Yan C, Gong X, Du M, and Shi Y (2014) Structure and mechanism of a eukaryotic transmembrane ascorbate-dependent oxidoreductase, Proc Natl Acad Sci U S A 111, 1813–1818. [PubMed: 24449903]
11. Xia D, Esser L, Tang WK, Zhou F, Zhou Y, Yu L, and Yu CA (2013) Structural analysis of cytochrome bc1 complexes: implications to the mechanism of function, Biochim Biophys Acta 1827, 1278–1294. [PubMed: 23201476]
12. Zara V, Conte L, and Trumpower BL (2009) Biogenesis of the yeast cytochrome bc1 complex, Biochim Biophys Acta 1793, 89–96. [PubMed: 18501197]
13. Tikhonov AN (2014) The cytochrome b6f complex at the crossroad of photosynthetic electron transport pathways, Plant Physiol Biochem 81, 163–183. [PubMed: 24485217]
14. Ohgami RS, Campagna DR, McDonald A, and Fleming MD (2006) The Steap proteins are metalloreductases, Blood 108, 1388–1394. [PubMed: 16609065]
15. Kleven MD, Dlakic M, and Lawrence CM (2015) Characterization of a single b-type heme, FAD, and metal binding sites in the transmembrane domain of six-transmembrane epithelial antigen of the prostate (STEAP) family proteins, J Biol Chem 290, 22558–22569. [PubMed: 26205815]
16. Grunewald TG, Bach H, Cossarizza A, and Matsumoto I (2012) The STEAP protein family: versatile oxidoreductases and targets for cancer immunotherapy with overlapping and distinct cellular functions, Biol Cell 104, 641–657. [PubMed: 22804687]
17. Warkentin E, Mamat B, Sordel-Klippert M, Wicke M, Thauer RK, Iwata M, Iwata S, Ermler U, and Shima S (2001) Structures of F420H2:NADP+ oxidoreductase with and without its substrates bound, EMBO J 20, 6561–6569. [PubMed: 11726492]
18. Gauss GH, Kleven MD, Sendamarai AK, Fleming MD, and Lawrence CM (2013) The crystal structure of six-transmembrane epithelial antigen of the prostate 4 (Steap4), a ferri/cuprireductase, suggests a novel interdomain flavin-binding site, J Biol Chem 288, 20668–20682. [PubMed: 23733181]
19. Sendamarai AK, Ohgami RS, Fleming MD, and Lawrence CM (2008) Structure of the membrane proximal oxidoreductase domain of human Steap3, the dominant ferrireductase of the erythroid transferrin cycle, Proc Natl Acad Sci U S A 105, 7410–7415. [PubMed: 18495927]
20. Persechini A, McMillan K, and Masters BS (1995) Inhibition of nitric oxide synthase activity by Zn2+ ion, Biochemistry 34, 15091–15095. [PubMed: 7578122]
21. Slotboom DJ, Duurkens RH, Olieman K, and Erkens GB (2008) Static light scattering to characterize membrane proteins in detergent solution, Methods 46, 73–82. [PubMed: 18625320]
22. Kendrick BS, Kerwin BA, Chang BS, and Phil JS (2001) Online size-exclusion high-performance liquid chromatography light scattering and differential refractometry methods to determine degree of polymer conjugation to proteins and protein-protein or protein-ligand association states., Anal. Biochem 299, 136–146. [PubMed: 11730335]
23. Holmquist B, and Vallee BL (1973) Tryptophan quantitation by magnetic circular dichroism in native and modified proteins, Biochemistry 12, 4409–4417. [PubMed: 4750252]

24. Berka V, Palmer G, Chen PF, and Tsai AL (1998) Effects of various imidazole ligands on heme conformation in endothelial nitric oxide synthase, Biochemistry 37, 6136–6144. [PubMed: 9558353]
25. Dutton PL (1978) Redox potentiometry: determination of midpoint potentials of oxidation-reduction components of biological electron-transfer systems, Methods Enzymol 54, 411–435. [PubMed: 732578]
26. Velick SF, and Strittmatter P (1956) The oxidation-reduction stoichiometry and potential of microsomal cytochrome, J Biol Chem 221, 265–275. [PubMed: 13345816]
27. McCoy JG, Ren Z, Stanevich V, Lee J, Mitra S, Levin EJ, Poget S, Quick M, Im W, and Zhou M (2016) The Structure of a Sugar Transporter of the Glucose EIIC Superfamily Provides Insight into the Elevator Mechanism of Membrane Transport, Structure 24, 956–964. [PubMed: 27161976]
28. Dawson JH, and Dooley DM (1989) Magnetic Circular Dichroism Spectroscopy of Iron Porphyrins and Heme Proteins, VCH Publishers, Inc., New York.
29. Schunemann V, Trautwein AX, Illerhaus J, and Haehnel W (1999) Mossbauer and electron paramagnetic resonance studies of the cytochrome bf complex, Biochemistry 38, 8981–8991. [PubMed: 10413471]
30. Tsai A-L, and Palmer G (1982) Purification and characterization of highly purified cytochrome b from complex III of Baker's yeast, Biochim. Biophys. Acta 681, 484–495. [PubMed: 6289886]
31. Vicente JB, Justino MC, Goncalves VL, Saraiva LM, and Teixeira M (2008) Biochemical, spectroscopic, and thermodynamic properties of flavodiiron proteins, Methods Enzymol 437, 21–45. [PubMed: 18433621]
32. Urich T, Coelho R, Kletzin A, and Frazao C (2005) The sulfur oxygenase reductase from Acidianus ambivalens is an icosatetramer as shown by crystallization and Patterson analysis, Biochim Biophys Acta 1747, 267–270. [PubMed: 15698962]
33. Lambeth JD, Kawahara T, and Diebold B (2007) Regulation of Nox and Duox enzymatic activity and expression, Free Radic Biol Med 43, 319–331. [PubMed: 17602947]
34. Panday A, Sahoo MK, Osorio D, and Batra S (2015) NADPH oxidases: an overview from structure to innate immunity-associated pathologies, Cell Mol Immunol 12, 5–23. [PubMed: 25263488]
35. Grunewald TG, Diebold I, Esposito I, Plehm S, Hauer K, Thiel U, da Silva-Buttkus P, Neff F, Unland R, Muller-Tidow C, Zobywalski C, Lohrig K, Lewandrowski U, Sickmann A, Prazeres da Costa O, Gorlach A, Cossarizza A, Butt E, Richter GH, and Burdach S (2012) STEAP1 is associated with the invasive and oxidative stress phenotype of Ewing tumors, Mol Cancer Res 10, 52–65. [PubMed: 22080479]

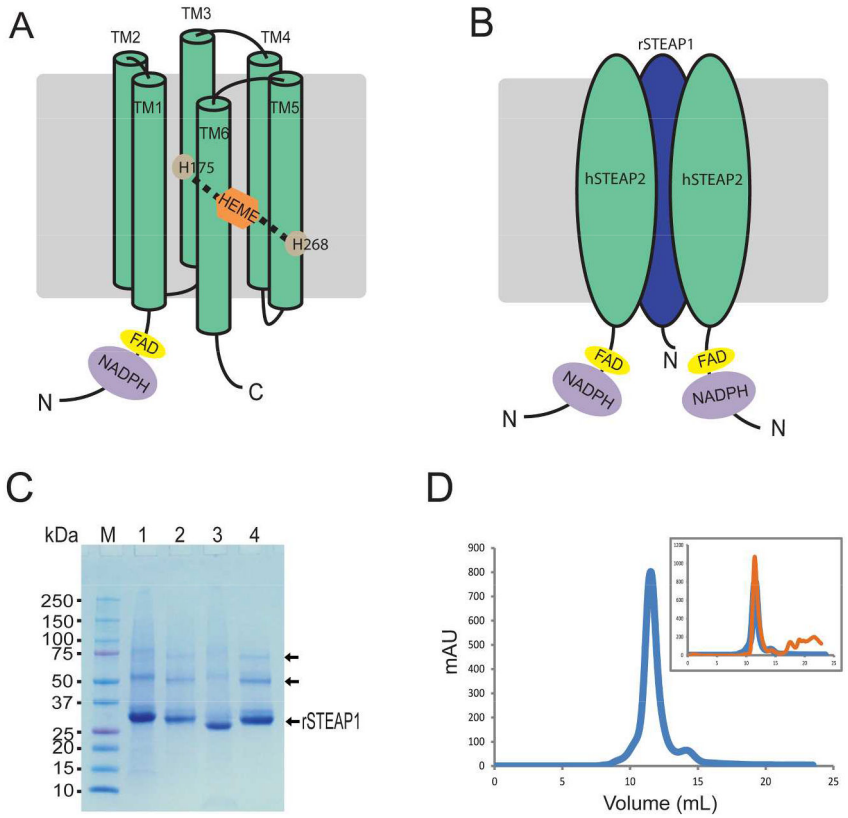

Figure 1.

Predicted membrane topology and purification of rSTEAP1. Predicted membrane topography of STEAP1 – 4 (A) and one of the two possible heterotrimeric assemblies between STEAP1 and STEAP2 (B). Different from STEAP1, STEAP2 – 4 have an extra N-terminal cytosolic domain predicted to bind NADPH and FAD. (C) SDS-PAGE gel analysis of the rSTEAP1 purification. M, molecular weight maker; lane 1, rSTEAP1-bound Co^{2+} chelating resin; lane 2, rSTEAP1 released from the Co^{2+} chelating resin by TEV; lane 3, Co^{2+} chelating resin after TEV treatment; lane 4, rSTEAP1 eluted from the size-exclusion column. The arrows indicate rSTEAP1 in monomeric (indicated by “rSTEAP1”), dimeric and trimeric states. (D) Size-exclusion chromatogram showing a sharp and symmetrical peak of rSTEAP1. Inset, FPLC elution profile of of MalT from *Bacillus cereus* (orange) overlayed on that of rSTEAP1 (blue).

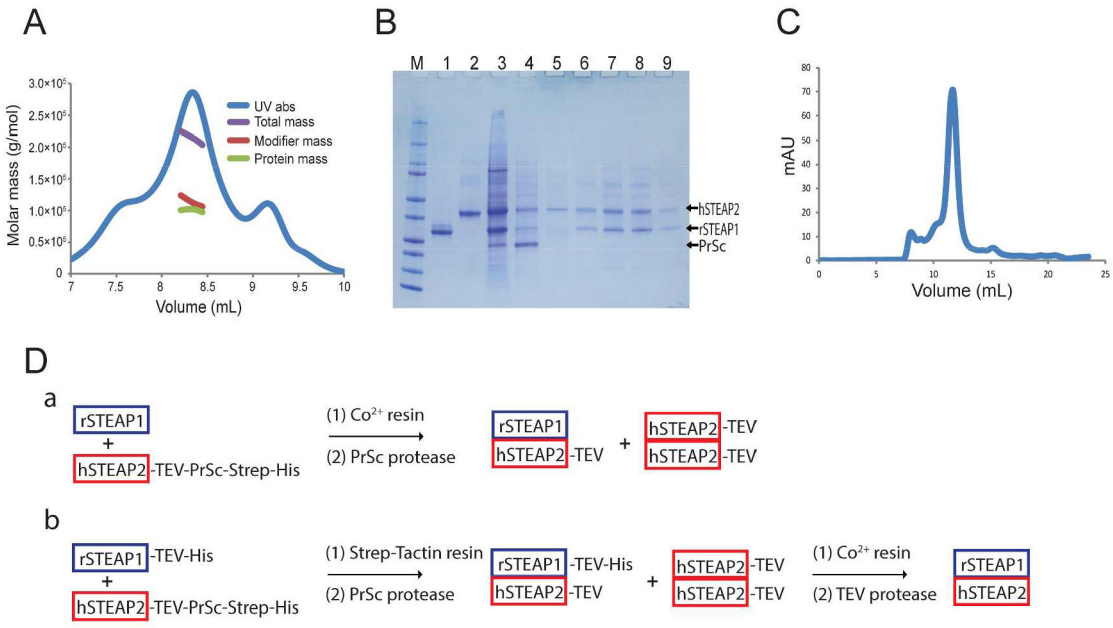

Figure 2.

Oligomeric state of rSTEAP1. (A) SEC-MALS analysis of rSTEAP1. The absorbance (blue) is shown versus the elution volume (x-axis). The total mass (protein + micelle, purple) and the deconvoluted masses of modifier (micelle, red) and protein (green) are indicated by the y-axis. The mass of the protein is ~110 kDa. (B) SDS-PAGE gel analysis of STEAP1 and STEAP2 co-expression: M, molecular weight maker; lane 1, rSTEAP1 (the light shadow above the main band may be due to different extent of glycosylation); lane 2, hSTEAP2 (~56kDa); lane 3, co-expression rSTEAP1-NT and hSTEAP2-TPSH treated with TEV after absorbed onto Co^{2+} chelating resin; lane 4, co-expression of rSTEAP1-TH and hSTEAP2-TPSH, treated by PrSc protease after binding to Strep-Tactin resin; lane 5, TEV treatment of the sample in lane 4 after its binding to Co^{2+} chelating resin; lanes 6 – 9, serial fractions collected for the major eluted peak in size-exclusion chromatography of the protease released proteins in lane 3. The arrows mark the bands of rSTEAP1, hSTEAP2 and PrSc protease. (C) Size-exclusion chromatogram of the sample from lane 3 in (B). (D) The scheme of co-expression and purification of rSTEAP1 and hSTEAP2.

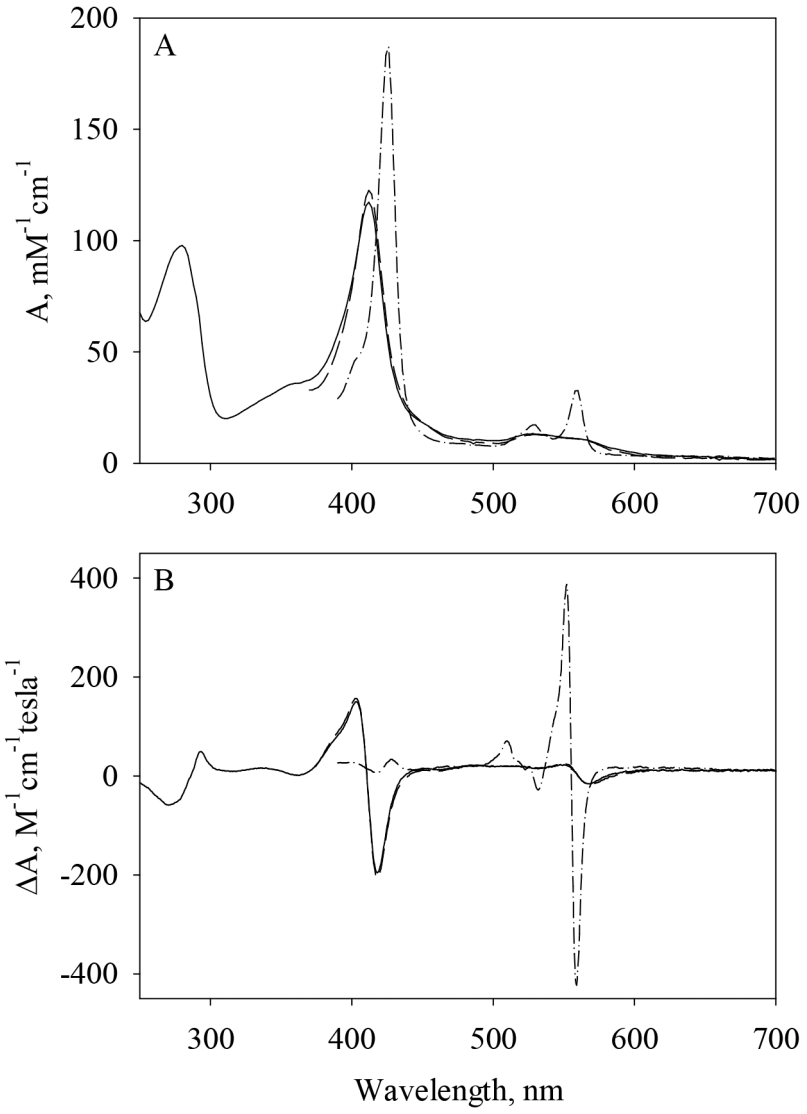

Figure 3.

UV-Vis absorption and MCD spectra of rSTEAP1. (A) Electronic absorption spectra and (B) MCD spectra of 3.3 μM ferric rSTEAP1 (solid line), ferric rSTEAP1 in the presence of 250 mM imidazole (dashed line) and ferrous rSTEAP1 (dash-dot line). The UV-Vis and MCD spectra are presented in extinction coefficients and difference extinction coefficients, respectively. In both panels, the spectra of rSTEAP1-Im under 370 nm and ferrous rSTEAP1 under 390 nm are omitted due to the distortion caused by the absorbance of excess imidazole and $Na_2S_2O_4$.

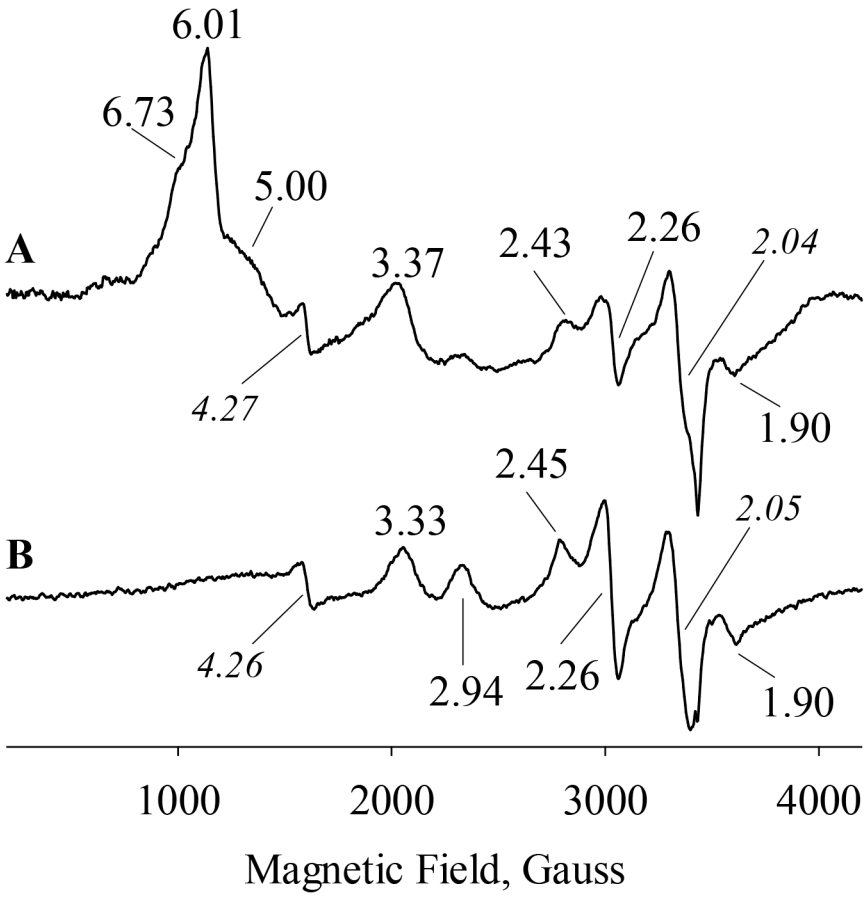

Figure 4.

EPR spectra of ferric rSTEAP1 and its complex with imidazole. EPR spectra of rSTEAP1 (83 μM) at 10 K without (A) and with the presence of 250 mM imidazole (B). The g values are labeled. Signal at g = 4.27 is due to non-specific or “adventitious” iron. Signal at g = 2.04 may also be contributed by unspecified radical(s).

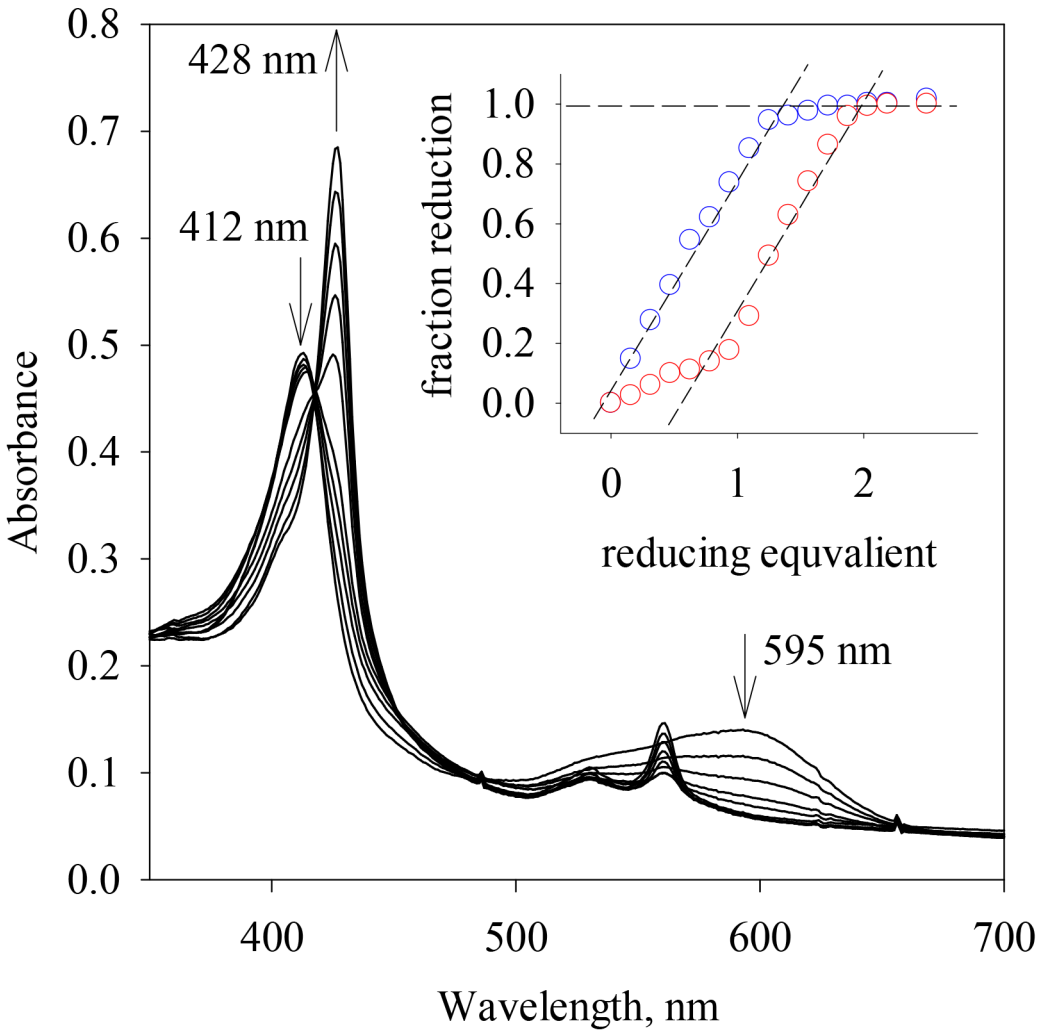

Figure 5.

Stoichiometric titration of rSTEAP1. The spectral changes during the titration of 4 μM rSTEAP1 with $Na_2S_2O_4$ in the presence of 4 μM indigo. The reduction/oxidation of heme was monitored by following the Soret absorptions of ferric and ferrous rSTEAP1 at 412 and 428 nm. The spectral changes of redox mediator indigo were monitored at 595 nm. The arrows indicate the directions of the spectral changes. Inset, the fractional reduction of indigo (blue circle) and rSTEAP1 (red circle) after each addition of $Na_2S_2O_4$. The dashed lines provide the visual guidance.

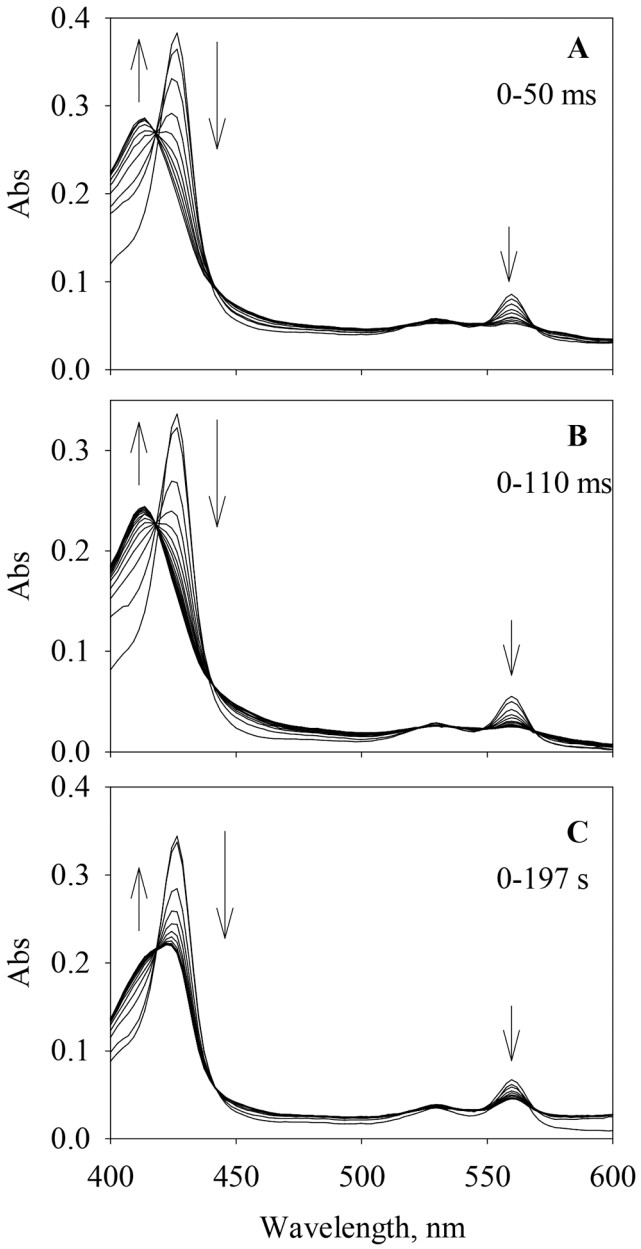

Figure 6.

Spectral changes during the reactions of ferrous rSTEAP1 with ferric or cupric ion complexes. Spectral changes in the anaerobic reactions of (A) 1.9 μM ferrous rSTEAP1 with 250 μM Fe^{3+}•EDTA (0 – 20 ms); (B) 1.8 μM ferrous rSTEAP1 with 250 μM Fe^{3+}•citrate (0 – 110 ms); and (C) 1.9 μM ferrous rSTEAP1 with 500 μM Cu^{2+}•EDTA (0 – 197 s). In each panel, the spectrum after ferrous rSTEAP1 mixed with anaerobic buffer is presented as the initial spectra at time 0 s. In each reaction, the first spectrum obtained and the time interval between every two spectra are (A) 1.28 ms/2.56 ms; (B) 1.28 ms/7.68 ms and (C) 0.65 s/ 13.1 s. The vertical arrows represent the directions of the absorbance changes in the Soret and α regions.

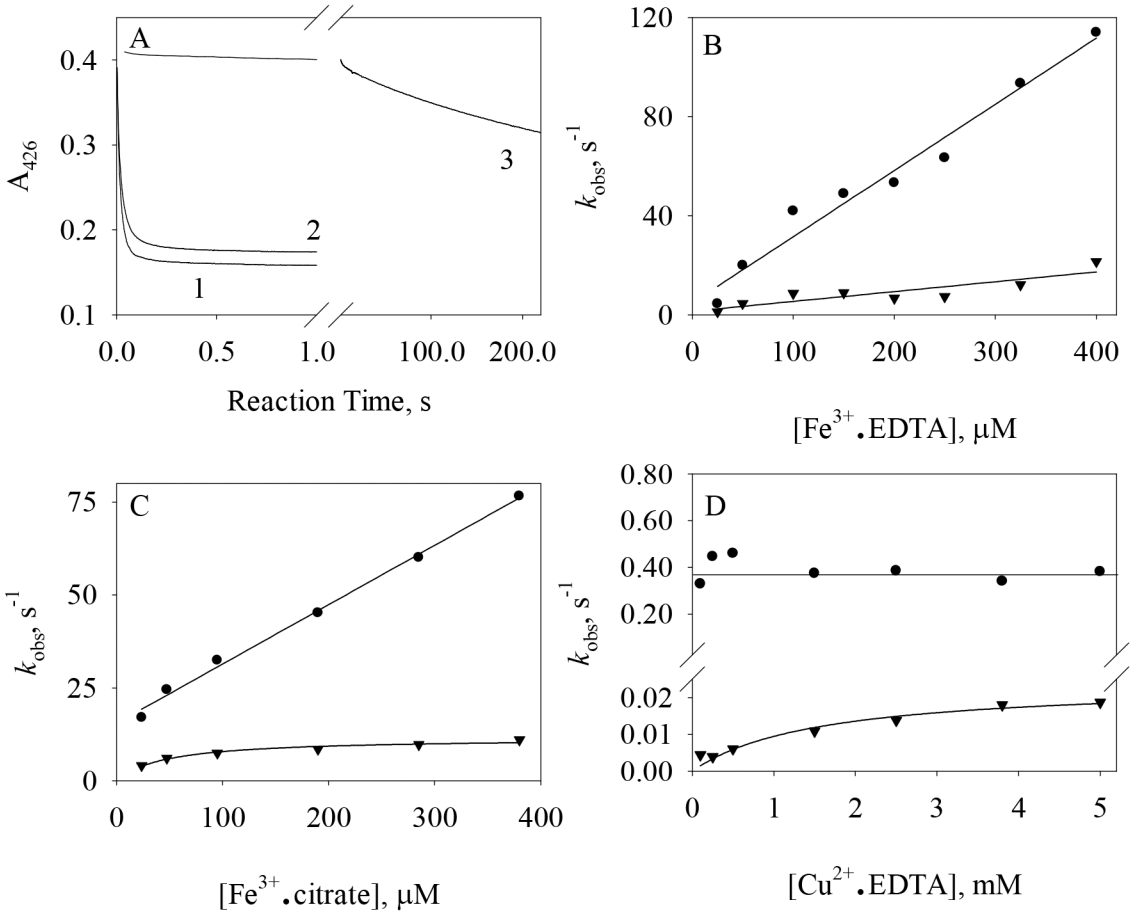

Figure 7.

Single wavelength stopped-flow kinetics of anaerobic reactions between ferrous rSTEAP1 and ferric or cupric ion complexes. (A) Time courses of A_{426} during the reactions between (1) 1.9 μM ferrous rSTEAP1 and 250 μM Fe^{3+}•EDTA; (2) 1.8 μM ferrous rSTEAP1 and 285 μM Fe^{3+}•citrate; and (3) 1.9 μM ferrous rSTEAP1 and 250 μM Cu^{2+}•EDTA. The time courses were all biphasic. The k_{obs} versus [metal ions] are presented in (B) Fe^{3+}•EDTA; (C) Fe^{3+}•citrate; and (D) Cu^{2+}•EDTA. Circle: k_{obs1} of fast phase; triangle: k_{obs2} of slow phase. The straight lines in (B) represent the linear fits of k_{obs1} and k_{obs2} versus [Fe^{3+}•EDTA], respectively. The straight line in (C) represents the linear fit of k_{obs1} versus [Fe^{3+}•citrate]; the lower curve represents the fit of k_{obs2} versus [Fe^{3+}•citrate] with Eq. [3]. The upper line in (D) indicates the averaged value for k_{obs1}, ~0.39 s^{-1}; the lower curve represents the fit of k_{obs2} versus [Cu^{2+}•EDTA] with the same function as above.

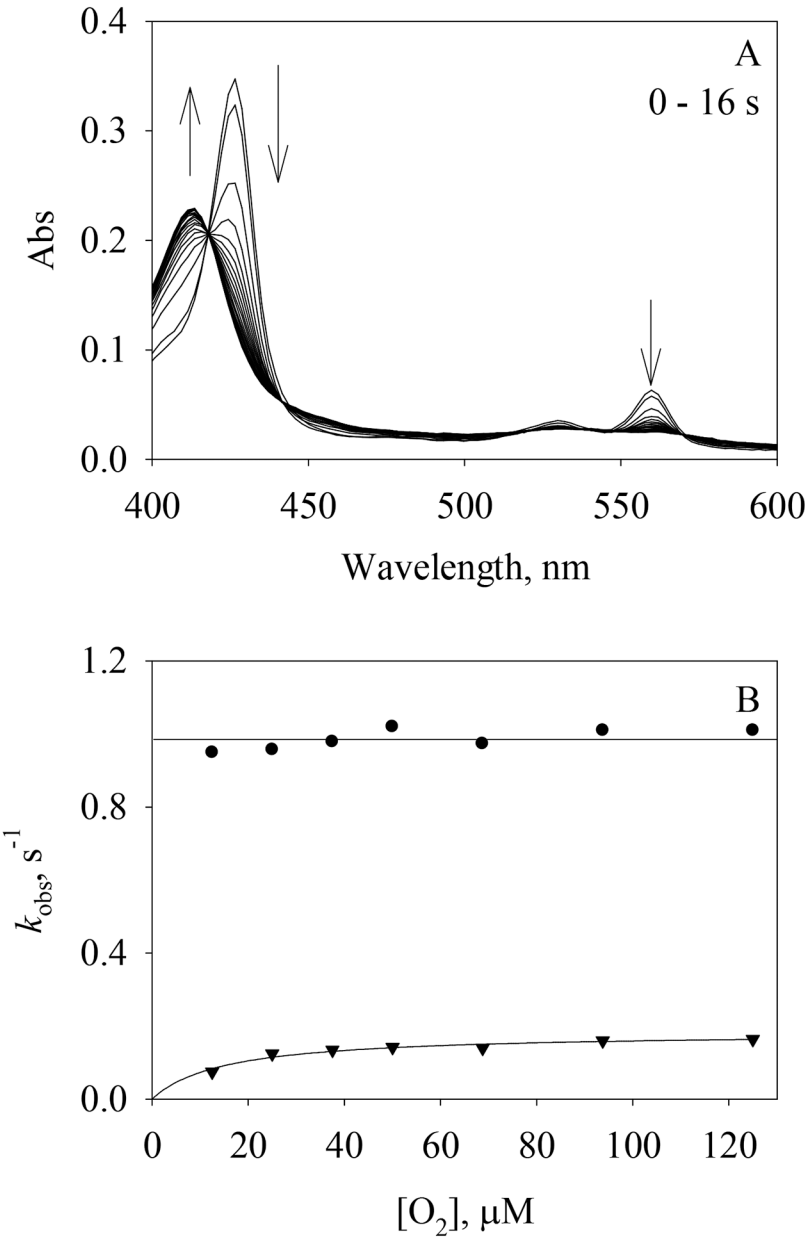

Figure 8.

Kinetics of the reactions between ferrous rSTEAP1 and O_2. (A) Spectral changes during the reactions of 1.9 μM ferrous rSTEAP1 with 120 μM O_2 (0 – 16.4 s). The spectrum after rSTEAP1 mixed with anaerobic buffer is presented as the initial spectra at time 0 s. The first spectrum after mixing with O_2 was obtained at 160 ms and the time interval between every two spectra is 0.82 s. The vertical arrows represent the spectral changes in Soret and α regions. (B) Dependence of A_{426} decaying rates, k_{obs}, versus $[O_2]$. The time courses of A_{426} exhibit biphasic decay at each $[O_2]$. The upper line represents the averaged value for k_{obs1}, ~ 0.9 s^{-1} (circle). The lower curve shows the fit for k_{obs2} (triangle) versus $[O_2]$ using Eq. [3].

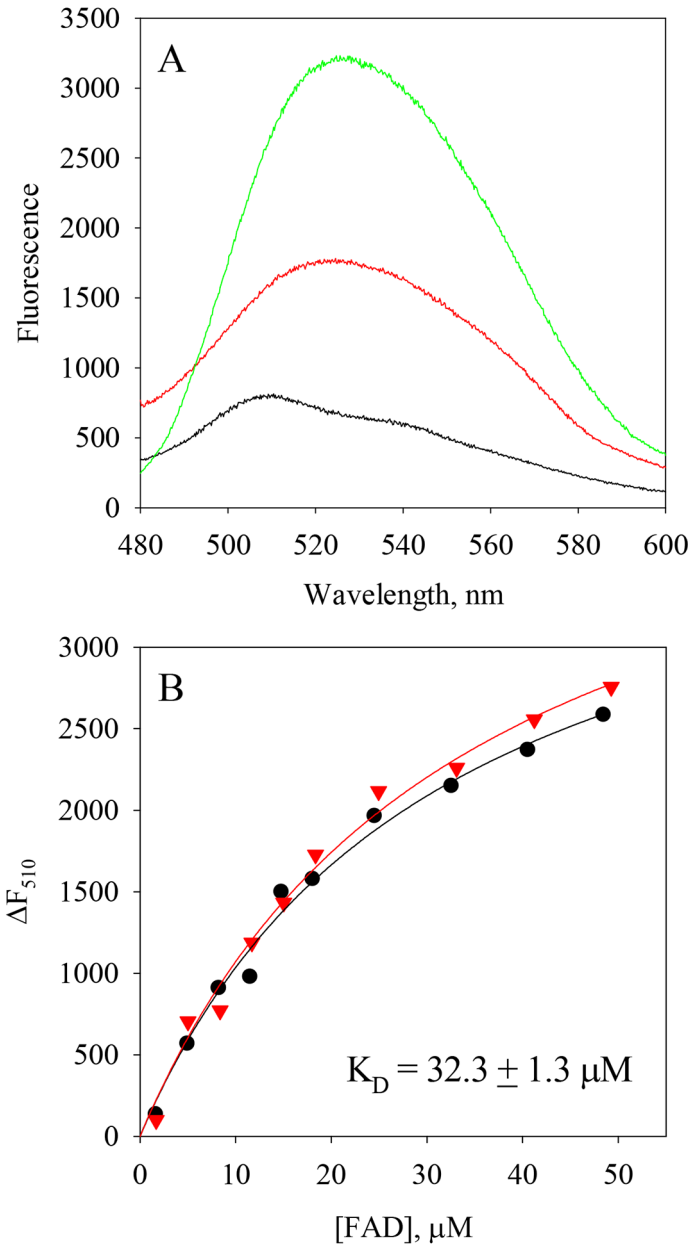

Figure 9.

Characterization of FAD binding in rSTEAP1. (A) Fluorescence spectra of 23.3 μM purified rSTEAP1 (black); FAD released from denatured rSTEAP1 (red) and 1 μM free FAD in buffer (green). (B) Two titrations of rSTEAP1 with FAD. The difference fluorescence at 510 nm, ΔF_{510}, was plotted versus [FAD] and the isotherms were fit with eq. [4]. [rSTEAP1] in the two titrations was 12.3 μM (black circles) and 11.5 μM (red triangles), respectively.